

Invariant Representation Driven Neural Classifier for Anti-QCD Jet Tagging

Taoli Cheng, Aaron Courville

Mila – Quebec Artificial Intelligence Institute, Montreal, QC H2S 3H1, Canada

Department of Informatics, Université de Montréal, Montreal, QC H3T 1J4, Canada

E-mail: chengtaoli.1990@gmail.com, aaron.courville@umontreal.ca

ABSTRACT: We leverage representation learning and the inductive bias in neural-net-based Standard Model jet classification tasks, to detect non-QCD signal jets. In establishing the framework for classification-based anomaly detection in jet physics, we demonstrate that with a *well-calibrated* and *powerful enough feature extractor*, a well-trained *mass-decorrelated* supervised neural jet tagger can serve as a strong generic anti-QCD jet tagger for effectively reducing the QCD background. Imposing *data-augmented* mass-invariance (decoupling the dominant factor) not only facilitates background estimation, but also induces more substructure-aware representation learning. We are able to reach excellent tagging efficiencies for all the test signals considered. In the best case, we reach a background rejection rate of 50 and a significance improvement factor of 3.6 at 50 % signal acceptance, with jet mass decorrelated. This study indicates that supervised Standard Model jet classifiers have great potential in general new physics searches.

Contents

1	Introduction	1
2	Methodology	3
2.1	Supervised Classifier in Anomaly Detection: an Experiment	3
2.2	Classifier-based Anomaly Identifier: General Approach	4
2.3	Improving Model Uncertainty Estimate	7
2.3.1	Deep Ensemble	7
2.3.2	OVA-AVA Combinational Classification	7
2.3.3	Distance-aware Uncertainty Estimate	8
3	Setup	8
3.1	Datasets	8
3.2	Neural Classifier	9
3.3	Training Settings	9
4	Results	10
4.1	Anomalous Jet Tagging	10
4.2	Mass Decorrelated Anomalous Jet Tagger	11
5	Discussion	16
6	Summary	17
A	Neural Architecture and Datasets	19
B	Additional Results	20

1 Introduction

Data-driven beyond Standard Model (SM) new physics search at the Large Hadron Collider (LHC) has been explored in the regime of autoencoders [1–5], latent variable models [6, 7], density estimation [8, 9], and weakly supervised classification [10, 11]. Though generative modelling has the advantage of not relying on signal examples or simulated data, it has been observed that even perfect density estimation can’t guarantee out-of-distribution (OoD) detection [12–14]. Similar phenomena have been observed and further studied in generative model based anomalous jet tagging [5, 7]. Variational Autoencoders trained on background QCD jets might assign even higher likelihood to non-QCD signal jets, casting doubt on the

robustness of these approaches. At the same time, a community-wide challenge [15] for simulated signal detection at the LHC turned out to be short of effective solutions despite the efforts in exploring different generative models including variational autoencoders (and variants) and flow-based models.

On the other hand, discriminative classifier based out-of-distribution detection [13, 16–23], being an alternative approach, has been well studied in the machine learning community and has a few advantages especially because of the outstanding capacity of deep neural networks. By incorporating task-aware inductive biases within the neural classifier, it increases out-of-distribution awareness and sensitivity compared with the generative counterpart. At the same time, it is shown that the classification-induced latent representations could be meaningful and generalizable across similar classification tasks [24]. Combining these threads (representation learning, cross-task transferability, and anomaly detection), we explore the potential of classification-induced representations for searching for new physics signals, and establish the framework for model training, inference, and evaluation.

More concretely, in the context of heavy resonance search, we explore the limit of utilizing low-level information equipped deep neural classifiers for anti-QCD jet tagging. This is based on the assumption that latent representations learned by the classifier captures useful information to distinguish between signals and background. Slightly different from classical OoD detection, here we leverage the classification as class-conditional OoD detection (i.e. QCD vs non-QCD classification).

The main building blocks include in-distribution (InD) training sets, representation extractors (physics-oriented jet classifiers), and anomaly detection scenario (anomaly score, OoD tagging strategy):

- **Datasets:** A well-designed and inclusive set of in-distribution classes fully leverages the representational power of deep neural nets and thus facilitates better OoD detection performance. Including all the boosted Standard Model jets within the LHC kinematic range equivalently injects the domain knowledge on particle types and underlying interactions, and expects best tagging efficiency.
- **Neural architecture:** On the one hand, modern, high-capacity neural architectures are crucial for effective classification and representation extraction. On the other hand, physics-friendly architectures induces more generalization ability, which is also an important ingredient for effective OoD detection. There are great efforts in the community to discover sophisticated physics-motivated architectures. This effort could be re-utilized for generic new physics search.
- **OoD identifier:** When the classifier is not directly trained with / exposed to OoD examples, we normally utilize post hoc OoD identifiers interfaced with the trained model to select anomalous events. The learned representations can be interfaced to an OoD identifier, either directly through the latent vectors, or via the classification predictions.

- Predictive uncertainty estimate: The calibration of neural classifiers [25, 26] and the uncertainty estimate provide better guarantees for real-world deployment of deep neural networks. Methods improving uncertainty estimate have been shown to help with OoD detection as well.

In model-independent heavy resonance search, decorrelating jet mass from a tagger [27–29] is desired to facilitate effective background estimation. In supervised jet tagging, mass decorrelation generally decreases tagging performance. However, from a different perspective, we show that a mass-decorrelated supervised jet classifier can serve as a generic anomalous jet tagger with outstanding performance. Imposing mass-invariance on the classification task turns out to enhance (subdominant) feature learning effectively.

We leverage boosted SM jets (QCD/W/Top) as in-distribution classes and use the learned representations to perform anti-QCD jet tagging. We test on hypothesized jets originating from new physics heavy resonances. Regarding strategies to improve uncertainty estimate, we employ methods including deep ensembling, one-vs-all and all-vs-all combinational softmax probability and distance-preserving Gaussian Process. At inference time, to identify non-QCD jets, we use anomaly scoring functions based either on the softmax probability of being non-QCD or on the latent distance to QCD jets. Despite the fact that supervised neural classifiers are designed for specific classification tasks, we demonstrate that a mass-decorrelated supervised jet classifier can act as an effective generic anti-QCD tagger.

This paper is organized as follows: in Section 2, we depict our schematics and present the methodology. We present a QCD/W classifier viewed as an anomaly detector and reveal the potential of a mass-decorrelated jet classifier serving as a generic anti-QCD tagger. Experimental setup (including datasets, neural architecture, and training settings) is introduced in Section 3. Anomaly detection performance without mass-decorrelation is recorded and analyzed in Section 4. Then the mass correlation effects and mass-decorrelated anti-QCD tagger are investigated. In Section 5, we comparatively discuss anomalous jet tagging thematics in discriminative models vs generative models. Finally in Section 6, we summarize this work and present the conclusions.

2 Methodology

2.1 Supervised Classifier in Anomaly Detection: an Experiment

As an illustrative experiment, we first present a simple Standard Model jet classifier serving as an anomalous jet tagger (experimental details can be found in App. A and Sec. 3). As shown in Table 1, an accurate QCD/W jet classifier reaches an Area Under the Receiver Operating Characteristic Curve (AUC) of 0.979. If we interpret the softmax probability $p_{\text{QCD}} = p(y = 0|\mathbf{x})$ as the probability of a jet being QCD-like, we can leverage the QCD/W neural classifier as an anti-QCD jet tagger. However, if we directly identify jets with a high non-QCD score $-p_{\text{QCD}}$ (equivalently p_W since for a QCD/W classifier we have $p_{\text{QCD}} + p_W = 1$)

as inclusive non-QCD jets, testing on discriminating top jets against the QCD background gives an AUC of 0.783.

Surprisingly, for the mass-decorrelated ¹ QCD/W classifier, we see promising anti-QCD tagging performance of improved tagging efficiency. (This observation also applies to a QCD/Top classifier.) Though the data are generated under different settings, we find that our mass-decorrelated QCD/W classifier gets an AUC of 0.861 for top samples from Ref. [1]. This is encouraging compared with the AUCs reported there (ranging from 0.63 to 0.78 depending on the decorrelation strength). Remembering that the result is already under distribution shift, we expect even improved performance if the model is trained on data with the same setting as in [1]. In comparison, the un-decorrelated classifier with predominant correlation with jet mass will strongly refer a jet with mass close to that of the in-distribution W jets (80 GeV) as non-QCD jets, while suppressing other discriminative factors.

This experiment shows great potential in utilizing the supervised jet classifier as a generic anti-QCD jet tagger. In the following we will explore the limit of neural jet classifiers performing in OoD detection.

Model	W	Top	Top from [1]	Model	Top	W
QCD/W	0.979	0.783	0.776	QCD/T	0.966	0.891
QCD/W (\mathcal{M})	0.958	0.860	0.861	QCD/T (\mathcal{M})	0.876	0.915

Table 1. OoD detection performance in AUC for a (mass-decorrelated (\mathcal{M})) binary jet classifier with $-p_{\text{QCD}}$ as the anomaly score. **Left:** QCD/W classifier tested on Top; **Right:** QCD/T classifier tested on W.

2.2 Classifier-based Anomaly Identifier: General Approach

The general approach of employing supervised classifier as anomalous jet tagger is depicted in the schematic in Fig. 1. First we train a QCD/W/T 3-class classifier simply on all the in-distribution SM classes $\{(\mathbf{x}_i, y_i); i = 1, \dots, N\}$. When we employ the QCD/W/T 3-way classifier as an anomalous jet tagger, we take advantage of the subtle substructures, which are critical for discriminating a rich set of SM jets, thus possibly generalizable to identifying new signals. We take advantage of a powerful feature extractor ² for effective representation learning ($\mathbf{x} \mapsto \mathbf{h}(\mathbf{x})$). Post hoc anomaly scoring functions depending on the trained classifier are used for identifying non-QCD jets in the inference phase.

Fig. 2 shows the softmax simplex distribution for three different OoD signals. For in-distribution samples, they are expected to aggregate around the corners which has high classification confidence. While, for out-of-distribution samples, they are more randomly distributed on the simplex plane. More interestingly, mass-decorrelation induces new patterns

¹Mass decorrelation is achieved by data augmentation in the mass dimension. We mass-augment and resample the W jets to match the mass distributions of QCD and W. This procedure will be discussed in Sec. 3.

²In this study we employ a Graph Neural Net called ParticleNet. (Check Sec. 3 and App. A for details.)

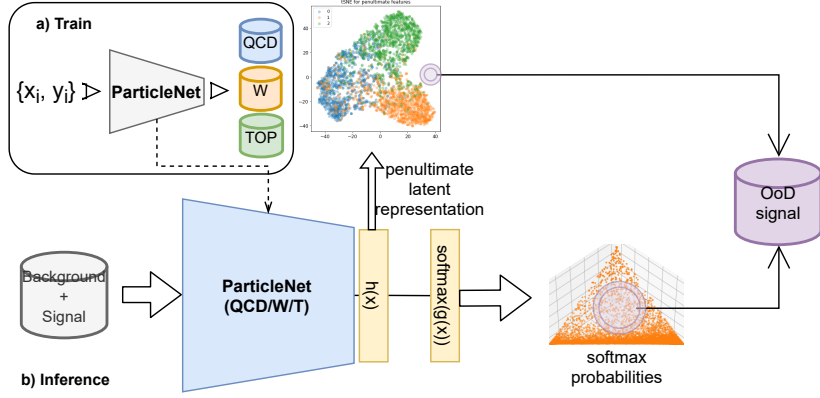


Figure 1. Schematic of neural classifier based anti-QCD jet tagging. The workflow consists of two steps. In the train step (a), we choose the *in-distribution classes* and the *feature extractor*. In the inference step (b), we design post hoc *anomaly scoring functions* operating on the trained classifier model for signal detection.

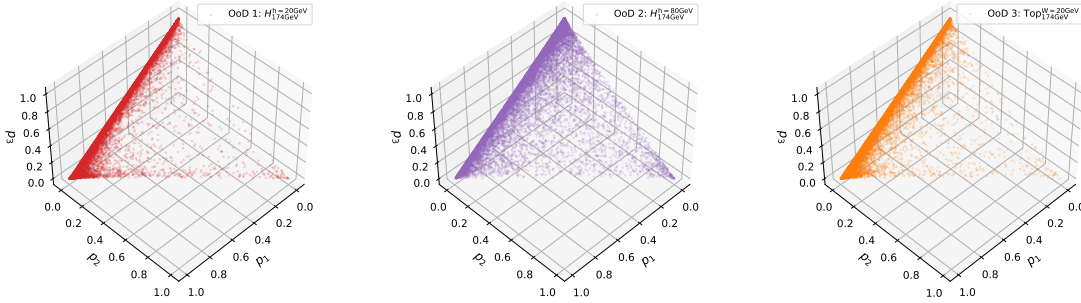


Figure 2. Softmax simplex of out-of-distribution classes within a QCD/W/T classifier.

in the softmax simplex (Fig. 3). Generally speaking, before mass-decorrelation, the OoD examples are more InD1- and InD3-like. With mass-decorrelation, the distributions change drastically, indicating a different representation pattern. We will see later in Sec. 4 how this results in effective signal detection.

In practice, we can either cast the anomalous jet tagging problem as a standard OoD detection problem (i.e. inclusively against all the SM jets), or reformulate it as a class-conditional anti-QCD tagging problem. In the context of new physics search, we have highly-imbalanced experimental data depending on the hadronic nature of the LHC. Most of the background events are from QCD jet production processes. And other background processes can be effectively reduced or estimated. Thus in the following we will focus the study on the formulation of anti-QCD tagging (as illustrated in the experiment above).

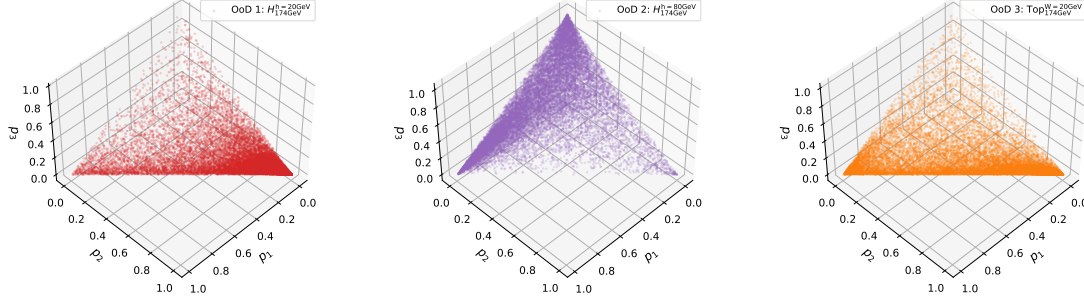


Figure 3. Softmax simplex of out-of-distribution classes within a mass-decorrelated QCD/W/T classifier.

$$\mathbf{x} \mapsto \mathbf{h}(\mathbf{x}); \mathbf{g}(\mathbf{x}) = \mathbf{W}\mathbf{h}(\mathbf{x}) + \mathbf{b}; p_k(\mathbf{x}) = \frac{\exp(\mathbf{g}_k(\mathbf{x}))}{\sum_{k'}^K \exp(\mathbf{g}_{k'}(\mathbf{x}))} \quad (2.1)$$

In principle, the anomaly scoring function can be composed with the predictive softmax probabilities ($p(\mathbf{x})$ in Eq. 2.1), the logits before the softmax activation ($\mathbf{g}(\mathbf{x})$), or the (penultimate) latent representation ($\mathbf{h}(\mathbf{x})$). For a well-calibrated model, the classifier prediction can be safely interpreted as the posterior probability. Thus we directly employ the predictive softmax probabilities as the anomaly score. However, as was argued in [30, 31], the softmax outputs are “label-overfitted” and thus likely to be mis-calibrated. This observation motivates the usage of the penultimate layer representations, with which we could instead measure density probabilities in the feature space and be free of the overconfidence problem caused by affine transformations. In the context of anti-QCD tagging, we compose (QCD) class-conditional scoring functions as follows:

- **Softmax probability based scoring function:** class-conditional *non-QCD* softmax probability $-p_{\text{QCD}}(\mathbf{x})$ with $p_{\text{QCD}} = p(y = 0 \mid \mathbf{x})$ (the minus sign accounts for the reverse in **anti-QCD** detection).
- **Representation based scoring function:** to directly measure the distance in latent space, we employ the Mahalanobis Distance (MD) [31, 32] in the penultimate layer, by seeing the classifier as a Gaussian Model. Normally we calculate the mean and covariance matrix (Eq. 2.2b) in the training set, and measure the distance (Eq. 2.2a) from the test datum to the target cluster.

$$\text{MD} = (\mathbf{h}(\mathbf{x}) - \mu)^\top \Sigma^{-1} (\mathbf{h}(\mathbf{x}) - \mu) , \quad (2.2a)$$

$$\text{with } \mu = \frac{1}{N} \sum_i^N \mathbf{h}(\mathbf{x}_i^{\text{train}}), \quad \Sigma = \frac{1}{N} \sum_i^N (\mathbf{h}(\mathbf{x}_i^{\text{train}}) - \mu)(\mathbf{h}(\mathbf{x}_i^{\text{train}}) - \mu)^\top \quad (2.2b)$$

2.3 Improving Model Uncertainty Estimate

As improving uncertainty estimate [25, 26, 33, 34] at the same time helps with OoD detection, we explore three different methods in this section.

2.3.1 Deep Ensemble

Deep ensemble [17] as a practical method for uncertainty estimation has been leveraged for OoD detection as well. Compared with Monte-Carlo Dropout [35], it provides a more convenient protocol for uncertainty estimation. For classification problems, as indicated in Eq. 2.3, an ensemble model is well-approximated with averaging the predictive probabilities of M individually trained classifiers $p^{(m)}(y|\mathbf{x}, \theta)$.

$$p(y|\mathbf{x}, D) = \mathbb{E}_{p(\theta|D)}[p(y|\mathbf{x}, \theta)] \simeq \frac{1}{M} \sum_{m=1}^M p^{(m)}(y|\mathbf{x}, \theta) \quad (2.3)$$

2.3.2 OVA-AVA Combinational Classification

In the training of a classifier-based anomaly detector, the all-vs-all (AVA) classification might have the downside that the decision boundary is not informative enough, i.e. the decision boundary is not fully aligned with the data manifold boundaries. In the setting of a closed softmax probabilistic simplex, OoD examples as well as the InD samples are restricted to the plane. When OoD detection is fully driven by the decision boundary, it may lead to mis-specification and high detection error. One way to amend this is to combine one-vs-all (OVA) binary classification with all-vs-all classification [23, 36]. The multiplicative combination of the OVA and AVA probabilities (*pseudo-probability* in the sense that it's not an actual probability in theory) is then used as the anomaly scoring function as in Eq. 2.4, where $p^{k-\text{OVA}}(\mathbf{x})$ denotes the one-class probability of the k -th OVA neural classifier and $p_k^{\text{AVA}}(\mathbf{x})$ denotes the softmax probability for the k -th in-distribution class from the AVA classifier for datum \mathbf{x} .

$$p_k^{\text{OVA-AVA}}(\mathbf{x}) = p^{k-\text{OVA}}(\mathbf{x}) \times p_k^{\text{AVA}}(\mathbf{x}) , \quad (2.4a)$$

$$\text{with } p^{k-\text{OVA}}(\mathbf{x}) = p(y = 1|\mathbf{x}, \theta_k), \quad p^{k-\text{OVA}}(\mathbf{x}) = p(y = k|\mathbf{x}, \theta) \quad (2.4b)$$

In Fig. 4, we show the softmax probability simplex for one OoD class from a trained classifier. The OvA factor brings InD and OoD examples even further apart. There are two forces within this action: 1) the all-vs-all classifier pulls OoD data points towards the center (uniform softmax distribution); 2) the one-vs-all classifiers pulls OoD points away from the softmax plane towards the origin. At the same time, ideally for in-distribution classes, $p^{k-\text{OVA}}(\mathbf{x}_{\text{InD}})$ and $p_k^{\text{AVA}}(\mathbf{x}_{\text{InD}})$ both approach 1 for the k -th corresponding class. This will result in better separation between InD and OoD data.

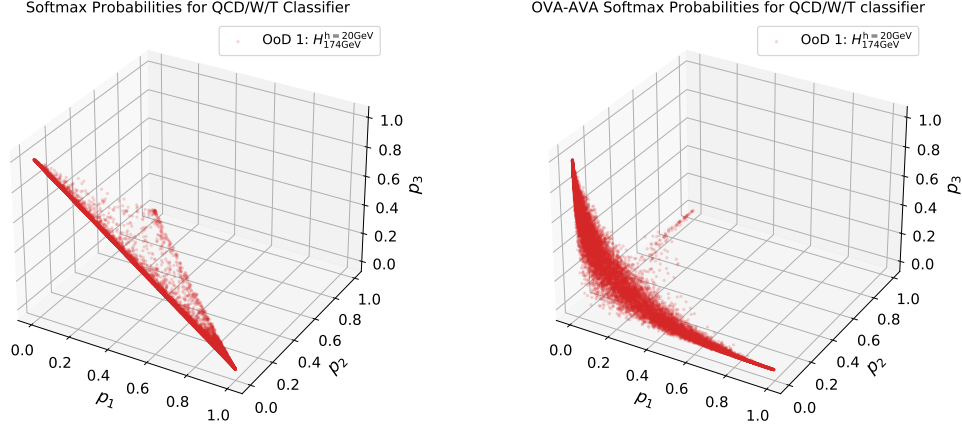


Figure 4. Softmax probabilities from the combined classification scenario.

2.3.3 Distance-aware Uncertainty Estimate

ReLU based networks could be brittle for having high predictive confidence even at OoDs far away from InD samples. It was proved that RBF networks can mitigate this problem [30]. Gaussian Process (GP) with a RBF kernel has the property of input distance awareness [37], in the sense that RBF kernels will have uniform predictions ($p(y|\mathbf{x}) \sim \frac{1}{K}$) for far OoDs.

In the same spirit, distance-aware uncertainty estimates could be achieved by a Spectral Normalized Gaussian Process (SNGP) [22] with two main ingredients: 1) the output layer replaced with a Gaussian Process with the RBF kernel

$$\mathbf{K}_{ij} = \exp(-\|\mathbf{h}(\mathbf{x}_i) - \mathbf{h}(\mathbf{x}_j)\|^2/2) ; \quad (2.5)$$

2) distance-preserving spectral normalization [38]. Spectral normalization is used to control the Lipschitz constant of the classifier by constraining the spectral norm layer by layer. Combining with the Gaussian Process output layer, distance between instances are expected to be well conserved. In practice, the output Gaussian Process is implemented with Laplace Approximation to the posterior approximated with Random Fourier Features (RFFs) [37].

3 Setup

3.1 Datasets

Training Sets The training set consists of boosted Standard Model QCD, W , and top jets with $p_T \in [550, 650]$ GeV. The events are generated with MadGraph [39] for 13 TeV LHC, with the production processes $pp \rightarrow jj$ ($j = u, d, c, s, g$) for QCD jets, $pp \rightarrow W' \rightarrow WZ$ ($m_{W'} = 1.25$ TeV) for W jets, and $pp \rightarrow Z' \rightarrow t\bar{t}$ ($m_{Z'} = 1.5$ TeV) for top jets. W boson and top quark are restricted to hadronic decaying modes (Z bosons are restricted to decaying into

neutrinos for collecting clean W jets). Generated events are then fed into `Pythia8` [40] and `Delphes` [41] for parton shower and fast detector simulation (no pile-up effects simulated). We take particle flow objects for jet clustering, with no jet trimming applied. All jets are then clustered with the `anti- k_T` algorithm [42] with cone size $R = 1.0$. We have 350,000 jets for each class, with 20% of the training samples serving as the validation set.

OoD Test Sets Test signal sets [43] are hypothetical new physics jet types including boosted scalar jets (4-prong) and altered top jets (3-prong). We borrow Two Higgs Doublet Models (THDMs) [44] to generate boosted Higgs jets with pair production ($pp \rightarrow HH$, $H \rightarrow h(bb)h(bb)$), where the light Higgs boson is in the $h \rightarrow b\bar{b}$ decay mode. We set $m_H = 174$ GeV with $m_h = 20, 80$ GeV to the Higgs bosons to express different shapes of “four-prongness”. In practice, we employ h_3 (requiring parton-level $p_T > 600$ GeV) in THDM as the heavy Higgs, and h_1 as the light Higgs. For the altered top jets, we rescaled the intermediate W mass to 20 GeV. A lighter W will generate different relative radiation patterns for the altered top jets. The production process is the same as for SM top jets.

All jets are again clustered using the `anti- k_T` algorithm with the cone size of $R = 1.0$. Test jet p_T s are confined to a narrow region [550, 650] GeV for a fair comparison. Each test set with refined p_T contains 20,000 samples.

Preprocessing and Input formats All jets are preprocessed following the procedure in Ref. [7], including centering and rotating in the (η, ϕ) plane to align the jet principal axes. The first 100 jet constituents with the highest p_T s are selected as DNN inputs with coordinates $\{(\log E_i, \log p_{Ti}, \eta_i, \phi_i)\}_{i=1}^{100}$.

3.2 Neural Classifier

ParticleNet [45] is employed as the classifier architecture in this study. ParticleNet is a dynamic convolutional neural net based on k nearest neighbours of each jet constituent. It performs excellently in multiple jet classification tasks including QCD/Top, QCD/ W , and quark/gluon classification. Categorical cross-entropy ($-\sum_k^K y_k \log(p_k(\mathbf{x}))$) is used as the loss function for the QCD/ W /T 3-class classification. We adopt the same hyper-parameters and learning rate scheduling from [45] for standard training and the OVA-AVA scenario. The model is trained for 30 epochs with the Adam optimizer [46]. Convergence is ensured by a decreasing learning rate.

3.3 Training Settings

Deep Ensemble For classification tasks, deep ensembling practically amounts to training M models independently and averaging over the predictive probabilities. We train 10 independent models with random initial weights and data ordering for the ensemble model.

OVA-AVA In practice, we train a QCD/ W /T AVA 3-class classifier and a QCD/(W ,T) OVA binary classifier with the same training samples.

SNGP For the SNGP training, we re-optimized the learning rate and schedule based on the procedure in [47]. More experimental details can be found in App. A.

4 Results

We present the classifier-based anomalous jet tagging performance in this section. We first present the un-decorrelated tagger for generic jet tagging. Then we examine the mass decorrelation effect and its impact in OoD detection.

4.1 Anomalous Jet Tagging

At inference time, the trained classifiers are used to calculate anomaly scores to perform a binary classification on in-distribution QCD jets and OoD signal jets. By thresholding the post-hoc anomaly scores, we select jets with the highest scores and identify them as non-QCD signals. To facilitate model comparison and estimate the overall performance, we employ the Receiver Operating Characteristic (ROC) Curve and the Area Under the ROC Curve (AUC) as metrics.

As introduced in Section 2, we investigate different training strategies and model setups. We explore 1) Single Model, 2) Deep Ensemble with 10 independent runs, 3) OVA-AVA combinational model, and 4) Distance-aware SNGP model. The softmax probability based scoring function is simply calculated as $-p_{\text{QCD}}(\mathbf{x}) = -p(y = 0|\mathbf{x})$ while QCD jets are labelled in 0. As for the class-conditional Mahalanobis distance, we extract the penultimate layer representation $\mathbf{h}(\mathbf{x})$ and calculate the class mean and covariance matrix (Eq. 2.2b) with 100,000 in-distribution QCD training samples.

Scenario	Signal			
		$H_{174\text{GeV}}^{h=20\text{GeV}}$	$H_{174\text{GeV}}^{h=80\text{GeV}}$	$\text{Top}_{174\text{GeV}}^{W=20\text{GeV}}$
SingleModel	p_{QCD}	0.782 ± 0.004	0.872 ± 0.001	0.768 ± 0.004
	MD	0.840 ± 0.008	0.856 ± 0.006	0.815 ± 0.008
Ensemble10	p_{QCD}	0.786 ± 0.001	0.878	0.774 ± 0.001
OVA-AVA	p_{QCD}	0.784 ± 0.002	0.876 ± 0.001	0.772 ± 0.002
SNGP	p_{QCD}	0.786 ± 0.004	0.875 ± 0.001	0.777 ± 0.003
	MD	0.834 ± 0.005	0.860 ± 0.006	0.819 ± 0.005

Table 2. OoD detection AUCs for different model training strategies and anomaly scoring functions (p_{QCD} and Mahalanobis distance MD). Standard deviations are calculated from 10 random runs, except that for the Ensemble model we bootstrap for 5 times from 20 individual models. (In case of a too small (< 0.001) standard deviation, we omit it in the table.) For each test signal, the highest AUC is highlighted in bold.

AUCs for discriminating test signal against the QCD background are recorded in Table 2. Standard deviations are calculated from 10 independent runs with random initial weights

and data ordering. Corresponding ROC curves for the optimal scenarios are shown in Fig. 5. In summary, we have the following observations:

- We reach AUCs $\sim 0.8\text{--}0.9$ for all the test signals, corresponding to background rejection rates $1/\epsilon_B(\epsilon_S = 0.5) \sim 8.5 - 13.5$ and significance improvement factors $\epsilon_S/\sqrt{\epsilon_B} \sim 1.46 - 1.84$.
- Different scenarios have different sensitivity regions. The latent-representation-based scoring function outperforms the softmax-probability-based scoring function in 2 out of 3 test signals, while p_{QCD} performs slightly better for $H_{174\text{GeV}}^{h=80\text{GeV}}$. Relatively speaking, $H_{174\text{GeV}}^{h=20\text{GeV}}$ (it has two highly boosted subjets and thus is similar to a W jet) and $\text{Top}_{174\text{GeV}}^{W=20\text{GeV}}$ are closer to the in-distribution classes as indicated in Fig. 2. Thus we can approximately categorize them as Near-OoDs [48].
- The three improvement methods in the uncertainty estimate all slightly strengthen the tagging performance. It confirms that better uncertainty estimate helps with OoD detection.

Though not recorded here, we also observe that a better feature extractor (neural architecture with higher classification accuracy) comes along with better OoD detection performance (A Fully Connected Network (FCN) is employed for model comparison. Results can be found in Table 6 of App. B).

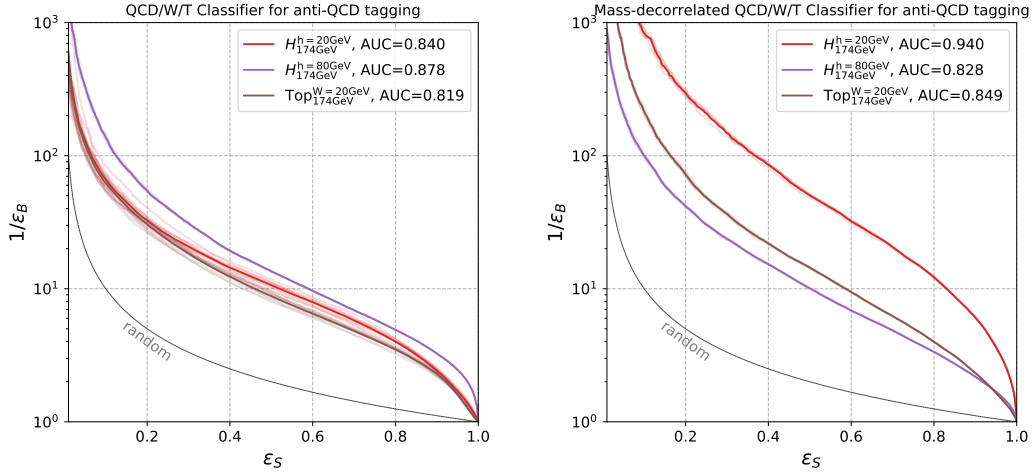


Figure 5. OoD ROC curves for un-decorrelated QCD/W/T classifier (*left*) and mass-decorrelated QCD/W/T classifier (*right*).

4.2 Mass Decorrelated Anomalous Jet Tagger

To better serve the general resonance searches and facilitate model comparison, we need to decorrelate jet mass from the anomaly scoring function. More concretely, a generic anomalous

jet tagger will confront the problem of mass sculpting (i.e. the tagger distorts the mass distribution of background jets). It has been considered a common problem in generic anomalous jet taggers. However, in this section, we argue that mass-decorrelation in the classifier-based approach augments OoD tagging efficiency, due to the inductive biases within the neural architecture and the classification task.

A mass-decorrelated jet tagger, generally, will have decreased tagging efficiency, since it blocks out the discriminative information of jet mass. For example, naive autoencoder-based anomalous jet taggers are strongly mass-correlated, resulting in over-simplified representations. Mass-decorrelated autoencoders, if not trained with augmenting strategies, in most cases have difficulties in preserving effective OoD detection performance. However, for neural classifier based anomalous jet tagging, the manifestation and the underlying mechanism are completely different: 1) Masses of the in-distribution classes will directly determine the mass correlation pattern. This might result in biased signal detection since jets with mass close to the peaks are given higher probabilities. 2) The predominant mass correlation will obscure effective representation learning for other relevant discriminative features such as jet substructure. 3) Mass-decorrelation in the classifier-based anomaly tagger plays a different role for anti-QCD tagging, compared to a supervised tagger or a generative anti-QCD tagger. It factorizes the mass-dependent part and the mass-independent part, and activates more generic features helpful in anomalous jet tagging.

To decorrelate jet mass from the classifier-function based anomaly scores, we employ the resampling strategy in [7]. By mass-augmenting and resampling the Standard-Model-like W and Top jets and matching the mass distributions to that of the QCD training samples, the classifier should be blind to the discriminative information from jet mass. Mass-rescaled Stand Model W jets (250,000) and Top jets ³ (160,000) are generated to span the full QCD mass spectrum. The neural architecture and the training procedure are the same as in the non-decorrelated version.

Mass correlation and decorrelation results are shown in Fig. 6 and 7 for p_{QCD} -based and Mahalanobis distance-based scoring functions. p_{QCD} is strongly shaped by in-distribution jet masses (peaking at W and Top masses) and perfectly mass-decorrelated when the classifier is trained with the mass-augmented training set. However, the latent Mahalanobis distance operates under a slightly different mechanism. We note that the non-decorrelated latent distance (*Top Panel* in Fig. 7) is weakly mass-correlated and is not strictly subject to data-imposed mass invariance. The softmax probability based scores are better regulated in this respect, since they are directly manifest in the training objective and trained with Maximum Likelihood Estimation. In comparison, the latent representations are more brittle and more reluctant regarding incorporating invariance within. This is however understandable because there are extra degrees of freedom ⁴ eaten in the softmax function.

The mass-decorrelated AUCs are recorded in Table 3, with the corresponding best case

³For smaller Top masses ($M_t \leq 80\text{GeV}$), the intermediate W boson mass is relatively rescaled.

⁴Translation in logits $g_k(\mathbf{x}) \rightarrow g_k(\mathbf{x}) + a$ will not change the softmax probabilities $p(\mathbf{x})$ (Eq. 2.1).

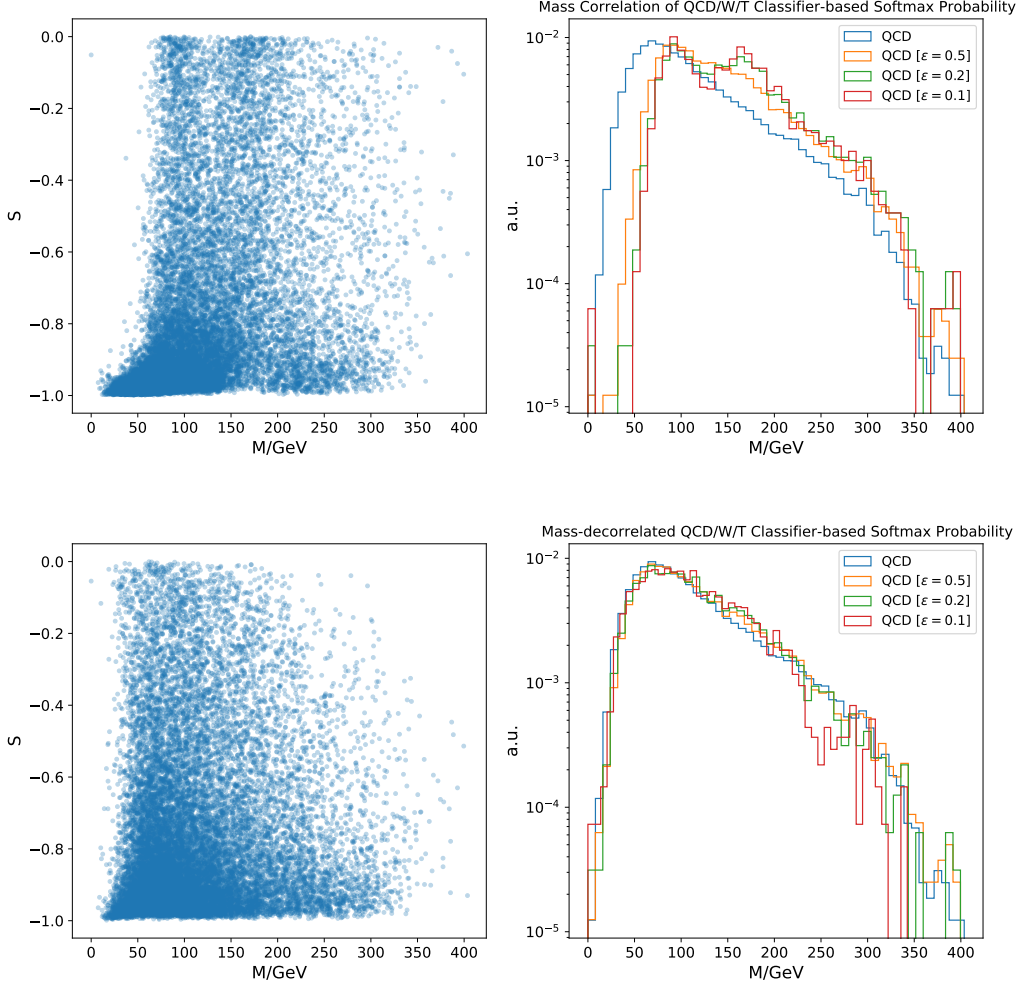


Figure 6. **Top:** Un-decorrelated model in p_{QCD} . **Bottom:** Mass-decorrelated model in p_{QCD} . **Left:** Correlation between jet mass M and the anomaly score. **Right:** Mass distributions for different background acceptance rate (ϵ).

ROC curves shown in the right panel of Fig. 5. We obtain promising signal tagging efficiency for all the test sets ($\text{AUC} \gtrsim 0.8$ with the background rejection rate $1/\epsilon_B(\epsilon_S = 0.5) \sim 15 - 50$). We also show the results from previous Outlier Exposed Variational Autoencoders (OE-VAE) [7] for model comparison. It's evident that the classifier-based approach outperforms OE-VAE.⁵

Overall, p_{QCD} performs better than MD, in both mass decorrelation and signal detection. Deep Ensemble with softmax probabilities is the best scenario here. Surprisingly, $H_{174\text{GeV}}^{h=20\text{GeV}}$

⁵We note that the encoding architecture in OE-VAE ((mainly dense layers)) is simpler than the architecture we used here. This leaves some room for further improvement in the OE-VAE approach.

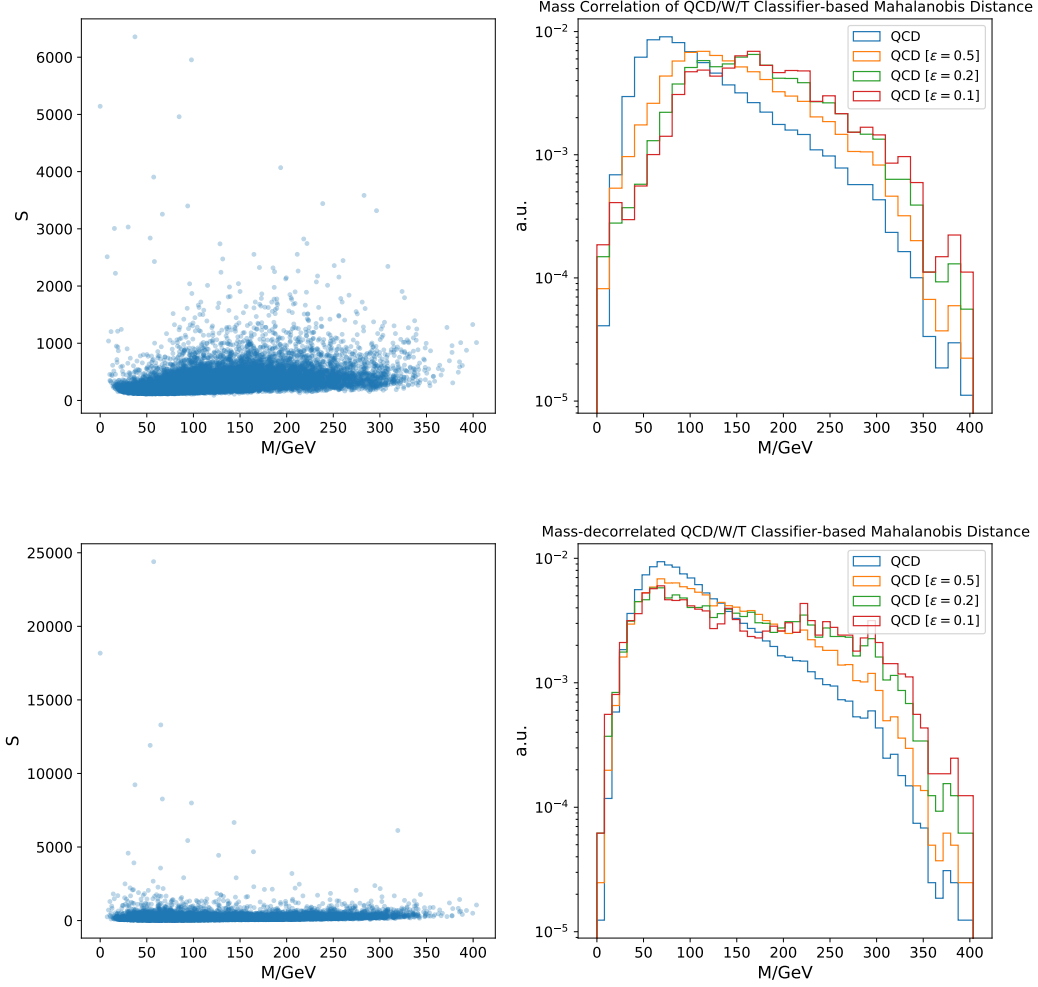


Figure 7. **Top:** Un-decorrelated model in Mahalanobis distance. **Bottom:** Mass-decorrelated model in Mahalanobis distance. **Left:** Correlation between jet mass M and the anomaly score. **Right:** Mass distributions for different background acceptance rate (ϵ).

even reaches an AUC of 0.940, which is exceptionally high for the current anomalous jet tagging benchmarks. At the signal acceptance rate of 50%, the background rejection rate reaches 51.0 and results in a significance improvement factor 3.6. At the same time, mass decorrelation yields a different performance pattern in the test sets. Intriguingly, $H_{174\text{GeV}}^{h=20\text{GeV}}$ and $\text{Top}_{174\text{GeV}}^{W=20\text{GeV}}$ have even higher AUCs than the corresponding un-decorrelated cases. This trend holds for both anomaly scores. Normally for in-distribution classes, the mass-decorrelated classifier will have slightly lower classification accuracy due to the deducted mass information. Since the masses of the OoD samples are close to one of the in-distribution classes (Top 174 GeV), the different patterns between InD and OoD classes indicates that mass-decorrelation

Signal		$H_{174\text{GeV}}^{h=20\text{GeV}}$	$H_{174\text{GeV}}^{h=80\text{GeV}}$	$\text{Top}_{174\text{GeV}}^{W=20\text{GeV}}$
Scenario				
OE-VAE		0.744	0.625	0.721
DisCo($\lambda = 100$)	p_{QCD}	0.595	0.740	0.648
	MD	0.645	0.745	0.681
SingleModel	p_{QCD}	0.937 ± 0.001	0.824 ± 0.001	0.846 ± 0.002
	MD	0.931 ± 0.005	0.757 ± 0.012	0.836 ± 0.008
Ensemble10	p_{QCD}	0.940	0.828	0.849
OVA-AVA	p_{QCD}	0.938 ± 0.001	0.825 ± 0.001	0.848 ± 0.001
SNGP	p_{QCD}	0.936 ± 0.001	0.820 ± 0.001	0.846 ± 0.001
	MD	0.920 ± 0.004	0.793 ± 0.006	0.833 ± 0.007

Table 3. OoD test AUCs under mass decorrelation for different model training strategies and anomaly scoring functions (p_{QCD} and Mahalanobis distance MD). Standard deviations are calculated from 10 random runs, except that for the Ensemble model we bootstrap for 5 times from 20 individual models. (In case of a too small (< 0.001) standard deviation, we omit it in the table.) For each test signal, the highest AUC is highlighted in bold. Results from mass-decorrelated Variational Autoencoders are shown as a reference. In addition, we also present a regularization based mass decorrelation method (DisCo) as comparison.

induces different representation useful for OoD detection. Mass-decorrelated tagger will benefit from the extra learning capacity while eliminating the predominant factor of jet mass. We view $H_{174\text{GeV}}^{h=20\text{GeV}}$ and $\text{Top}_{174\text{GeV}}^{W=20\text{GeV}}$ as Near-OoDs as introduced in the previous section. Thus for Near-OoDs, mass decorrelation generally increases the AUCs, while Far-OoDs (e.g. typical 4-prong $H_{174\text{GeV}}^{h=80\text{GeV}}$) have slightly lower AUCs compared to the non-decorrelated case.

However, we observe that the augmented performance could not be achieved with only decorrelating jet mass. In Table 3 we also present a regularization based mass decorrelation method: Distance Correlation (DisCo) [49] between the classifier predictions and jet masses is added to the cross-entropy loss as a regularization term. We choose the regularization strength $\lambda = 100$. The DisCo AUCs show that simply decorrelating mass doesn't result in improved OoD detection. The actual learning power is closely related to the data augmentation.

Data-augmented Mass Decorrelation Improves OoD Detection? It's intriguing that decorrelating jet mass with data augmentation results in more performant OoD detection. To better understand the underlying mechanism, we factorize the discriminative log-likelihood as

$$\log p(y|\mathbf{x}) = \log p_{\mathcal{M}}(y|\mathbf{x}) + \log p_M(y|\mathbf{x}) , \quad (4.1)$$

where $\log p_M(y|\mathbf{x})$ denotes the mass-dependent part and $\log p_{\mathcal{M}}(y|\mathbf{x})$ denotes the mass-independent part of the log-likelihood. Then we can view mass-decorrelation as a likelihood ratio approach [50], with the mass-dependent part is cancelled out. At the same time, data augmentation

in the mass dimension is inducing rich feature learning through the mass-independent part, and is expressing more subtle and weakly-correlated structures. In general resonance searches (e.g. bump hunt), we can scan the potential mass windows and thus brings back the mass dimension for identifying the mass bump. The eventual significance improvement factor is then further boosted as

$$\gamma = \gamma^{\text{pQCD}(\mathcal{M})} \cdot \gamma^M, \text{ with } \gamma \equiv \frac{\epsilon_S}{\sqrt{\epsilon_B}}, \quad (4.2)$$

where $\gamma^M > 1$. This echoes with the improved ABCD method for better targeted signal detection [51] and reveals the possibility of boosted model-independent search strategy.

5 Discussion

Extension in the Building Blocks We have established the general framework and demonstrated the potential of discriminative anti-QCD tagging. There are a few building blocks worth further exploring.

- Training datasets: currently we only train on the Standard Model boosted jets. It’s possible that the tagging performance and coverage could be further improved by systematically including other potential hypothetical new physics signals.
- Training strategy: we employ the simplest training in the current setting, which is not specifically designed for OoD detection. We expect even improved performance with advanced training techniques. Concurrently it’s worth exploring other training objectives .
- Domain adaptation: the supervised classifier depends on simulation data at the moment. In order to apply to real-data analysis with less distortion, it’s worth investigating the performance under distribution shifts and develop corresponding domain adaptation strategies.

Discriminative vs Generative Generative models for density estimation have been employed as one important approach for anomalous jet tagging. Despite that they could be a powerful tool for density estimation and accordingly be used for new signal detection, there are a few downsides associated. As one important motivation of our discriminative approach (or *CLassifier-based Anomaly Detection*, CLFAD), it is revealed that generative approach might assign higher likelihood to OoD examples than InD data. In contrast, the discriminative classifiers incorporate inductive biases that might help more effectively identify OoD instances ⁶. We summarize the comparison between these two approaches in Table 4.

⁶However, we don’t conclude that the classifier-based approach is completely guaranteed to be free from the mis-specification problem.

Discriminative	Generative
Representation-driven	Likelihood-driven, density estimation
Extra freedom of in-distribution classes	Sensitive to dominant correlations (in cases without further learning guidance)
Mass correlation depends on in-distribution classes	Strong mass correlation
Sensitive to jet types	Possibility of assigning high likelihood to OoD samples (observed in both computer vision and jet physics)
Sim-Data domain adaptation	Train directly on data

Table 4. Comparison of discriminative and generative approaches for generic anomalous jet tagging.

Briefly speaking, the generative approach is based on the density estimation ability of generative models, while the discriminative approach leverages more the representation learning aspect of neural feature extractors. There are great efforts in the community to push the limit of powerful neural jet classifiers. Taking advantage of these sophisticated architectures, targeted jet classifiers and general model-independent new physics search then support and motivate each other. The selection of simulated in-distribution classes acts in an important role in the discriminative approach, while we can train the generative models directly on data with negligible signal contamination (since they are supposed to be rare given the null results up to now). Both approaches demonstrate mass correlation, however, with different underlying mechanisms. As for the tagging performance and failure modes, CLFAD tends to have higher sensitivity to jet types especially the similarity to in-distribution classes. Generative models are under the risk of missing signals in a large scope (*perfect density estimation doesn't guarantee robust OoD detection*). Especially with mass-decorrelation, a (Variational) Autoencoder based tagger could fail drastically for most test signals. Finally, as mentioned above, the simulated training set of CLFAD might have deteriorated performance under distribution shift when deployed on real-data analysis. In this case, we need to additionally calibrate the neural models.

6 Summary

Despite the quick evolving of anomaly detection applications in LHC physics, the efforts are temporarily focused on a narrow track following generative models and density estimation. However, discriminative neural classifier is by itself an anomaly detector in the sense that it encodes discriminative information equipped with inductive biases to tag anomalies. In this work, we establish the framework for discriminative anomalous jet tagging.

In building the framework, we leverage the SM particles as known in-distribution jet classes to perform multi-class classification. The trained classifier is then employed as an anomaly detector, based on that a well-calibrated classifier will behave differently when confronted with OoD examples, either having higher predictive uncertainties, or having latent representations far away from in-distribution clusters. Furthermore, viewing the classifier as a feature extractor, the latent representations should preserve information for discriminating between in-distribution and out-of-distribution samples.

In practice, we simply optimize an edge-convolution based neural classifier for QCD/W/T multi-class classification. At the inference time, we investigated different anomaly scoring functions depending on the ingredients: 1) softmax probabilities and 2) penultimate latent vectors. The softmax probabilities are more stable and directly reflects the log-likelihood of the classifier. The latent representation is tricky in the sense that they could contain more information than softmax probabilities, but they might be vulnerable and brittle. Again, it has been discussed that model uncertainty estimate is linked with the performance of OoD detection. To better facilitate model uncertainty estimate, we explored three approaches: 1) deep ensemble, 2) all-vs-all classification combined with one-vs-all classification, and 3) spectral normalized Gaussian Process. To facilitate effective background estimation in general resonance search, we augment and resample the training sets to match the mass distributions of all the in-distribution classes. In addition, mass decorrelation has another effect in this setup. By eliminating the predominant factor jet mass in the learning process, the representation learning capacity is better exerted to manifest other discriminative factors.

For model evaluation, we employed hypothetical new physics particles as test OoD signals. AUCs and ROCs are used for measuring the overall OoD detection performance. We examined different scenarios, and from the experiments we observe that:

- For all the test signals, we are able to reach AUCs larger than 0.8, no matter with mass decorrelation or not.
- The data-augmented and mass-decorrelated SM jet classifier can serve as a powerful generic anti-QCD jet tagger, thanks to the augmented feature learning. In the best case, we are able to reach an AUC of 0.940 and a background rejection rate of 50 at 50% signal acceptance.
- The softmax probability based scoring functions are more stable compared with the latent representation based scoring functions. Due to the extra degrees of freedom, the latent Mahalanobis distance is less aware of data-imposed mass invariance. Overall, p_{QCD} with mass decorrelation is the scenario optimized for signal detection (high sensitivity and precise mass decorrelation).
- Higher classification accuracy (thus better feature extractor) and better uncertainty estimate help with OoD detection. Though in our case, the improvement is not as significant.

In summary, we establish a framework for neural classifier based anomaly detection in jet tagging for LHC new physics search. Tailored for effectively reducing the most copious QCD background at the LHC, we reframe the OoD detection problem as class-conditional anti-QCD tagging. We observe that, with three ingredients: 1) powerful feature extractor, 2) decent model calibration, and 3) data-imposed mass decorrelation, a classification-driven neural net can serve as a performant generic anti-QCD tagger. This observation paves for further studies for supervised classifier-based however model-independent new physics search.

Acknowledgments

This work is supported by IVADO Postdoctoral Research Funding. Part of this work has been presented at the 2021 Machine Learning for Jets Workshop.

A Neural Architecture and Datasets

We employ the base model of ParticleNet [45]. It consists of Edge Convolution blocks which convolve across 16 nearest neighbours in the (η, ϕ) plane. The Edge-Convolution features are aggregated by average pooling before being fed into the dense layers for classification. We follow the default settings (architecture and learning rate schedule) therein, if not specifically stated.

ParticleNet

Architecture Inputs $((2+2) \times 100) \rightarrow \text{EdgeConv}(64, 64, 64) \rightarrow \text{EdgeConv}(128, 128, 128) \rightarrow \text{EdgeConv}(256, 256, 256) \rightarrow \text{Dense}(256) \rightarrow \text{Softmax}(2)$

Hyper-parameters The learning rate is scheduled as: $3\text{e-}4$ (8) $3\text{e-}3$ (8) $4\text{e-}3$ (4) $5\text{e-}7$, where numbers in the brackets are interval epoch counts. The batch size is set to be 384.

SNGP Hyper-parameters For the SNGP models, we employ the hyper-parameters in Table 5.

Power Iteration	1
Spectral Norm Bound (c)	0.99
Gaussian Process Hidden Dimension (D_L)	1024
Length-scale Parameter (l)	1.0
L_2 Regularization	1e-6
Covariance Ridge Factor (r)	1.00
Covariance Discount Factor	0.999
Learning Rate	4e-5 (10) 4e-4 (10) 4e-5 (5) 1e-6

Table 5. SNGP hyper-parameters. We use linear decay to schedule the learning rate. We linearly increase the rate to the target value 4e-5 and then decrease it to the initial value 4e-5. Finally we decrease the rate to 1e-6, and train for a few more epochs to ensure convergence. Numbers in brackets are epochs taken to finish the rate transition.

B Additional Results

Fully Connected Network

Architecture Input(80) \rightarrow Dense(256, ReLU) \rightarrow Dropout(0.2) \rightarrow Dense(128, ReLU) \rightarrow Dropout(0.2) \rightarrow Dense(12, ReLU) \rightarrow Softmax(3)

Hyper-parameters The learning rate is scheduled as: 2.5e-4 (10) 2.5e-3 (10) 2.5e-4, where numbers in the brackets are interval epoch counts. The batch size is set to be 256.

Scenario	$H_{174\text{GeV}}^{h=20\text{GeV}}$	$H_{174\text{GeV}}^{h=80\text{GeV}}$	$\text{Top}_{174\text{GeV}}^{W=20\text{GeV}}$
FCN- p_{QCD}	0.715	0.857	0.742
FCN-MD	0.716	0.722	0.722

Table 6. OoD test AUCs for a Fully Connected Network.

References

- [1] T. Heimel, G. Kasieczka, T. Plehn, and J. M. Thompson, *QCD or What?*, *SciPost Phys.* **6** (2019), no. 3 030, [[arXiv:1808.08979](#)].
- [2] M. Farina, Y. Nakai, and D. Shih, *Searching for New Physics with Deep Autoencoders*, *Phys. Rev. D* **101** (2020), no. 7 075021, [[arXiv:1808.08992](#)].
- [3] A. Blance, M. Spannowsky, and P. Waite, *Adversarially-trained autoencoders for robust unsupervised new physics searches*, *JHEP* **10** (2019) 047, [[arXiv:1905.10384](#)].
- [4] B. Ostdiek, *Deep Set Auto Encoders for Anomaly Detection in Particle Physics*, [[arXiv:2109.01695](#)].
- [5] T. Finke, M. Krämer, A. Morandini, A. Mück, and I. Oleksiyuk, *Autoencoders for unsupervised anomaly detection in high energy physics*, *JHEP* **06** (2021) 161, [[arXiv:2104.09051](#)].
- [6] O. Cerri, T. Q. Nguyen, M. Pierini, M. Spiropulu, and J.-R. Vlimant, *Variational Autoencoders for New Physics Mining at the Large Hadron Collider*, *JHEP* **05** (2019) 036, [[arXiv:1811.10276](#)].
- [7] T. Cheng, J.-F. Arguin, J. Leissner-Martin, J. Pilette, and T. Golling, *Variational Autoencoders for Anomalous Jet Tagging*, [[arXiv:2007.01850](#)].
- [8] B. Nachman and D. Shih, *Anomaly Detection with Density Estimation*, *Phys. Rev. D* **101** (2020) 075042, [[arXiv:2001.04990](#)].
- [9] A. Hallin, J. Isaacson, G. Kasieczka, C. Krause, B. Nachman, T. Quadfasel, M. Schlaffer, D. Shih, and M. Sommerhalder, *Classifying Anomalies THrough Outer Density Estimation (CATHODE)*, [[arXiv:2109.00546](#)].
- [10] J. H. Collins, K. Howe, and B. Nachman, *Anomaly Detection for Resonant New Physics with Machine Learning*, *Phys. Rev. Lett.* **121** (2018), no. 24 241803, [[arXiv:1805.02664](#)].
- [11] **ATLAS** Collaboration, G. Aad et al., *Dijet resonance search with weak supervision using $\sqrt{s} = 13$ TeV pp collisions in the ATLAS detector*, *Phys. Rev. Lett.* **125** (2020), no. 13 131801, [[arXiv:2005.02983](#)].

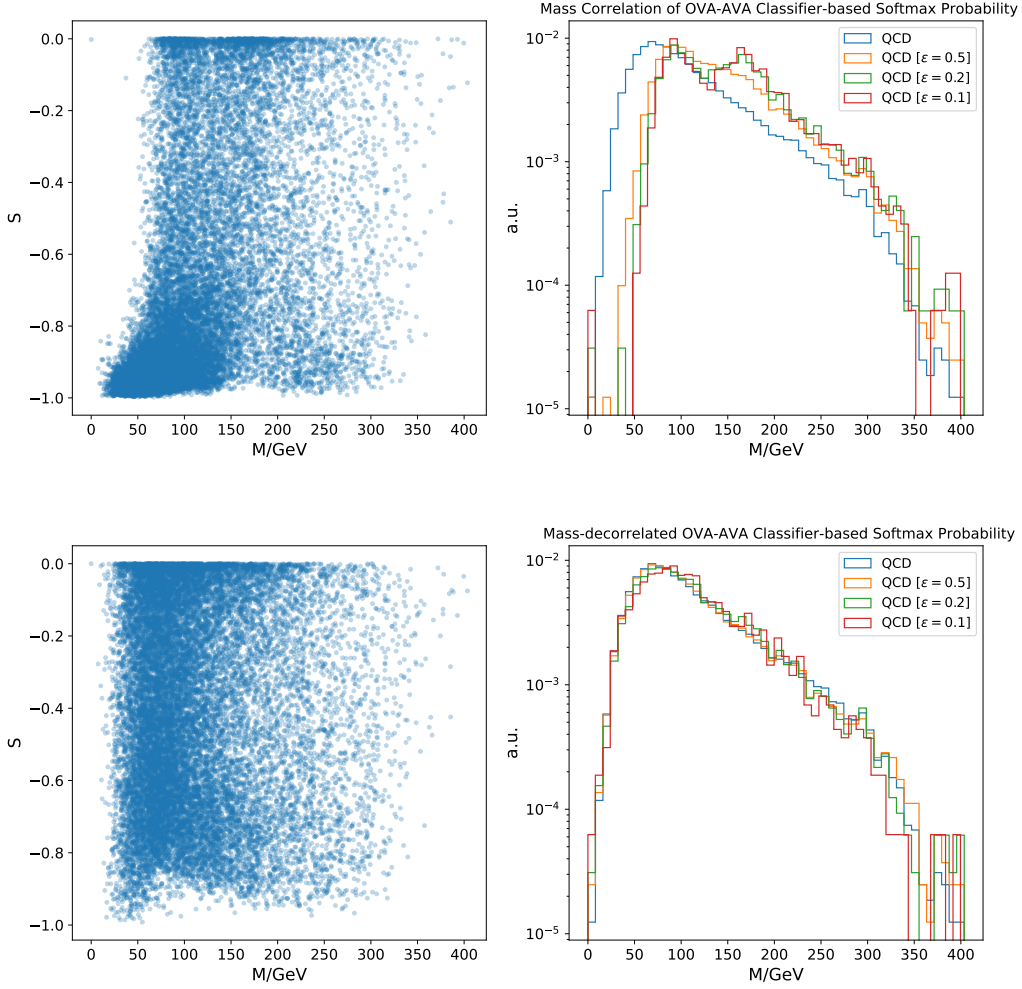


Figure 8. OVA-AVA Model. **Top:** Un-decorrelated model in p_{QCD} . **Bottom:** Mass-decorrelated model in p_{QCD} . **Left:** Correlation between jet mass M and the anomaly score. **Right:** Mass distributions for different background acceptance rate (ϵ).

- [12] E. Nalisnick, A. Matsukawa, Y. Whye Teh, D. Gorur, and B. Lakshminarayanan, *Do Deep Generative Models Know What They Don't Know?*, *arXiv e-prints* (Oct., 2018) [arXiv:1810.09136](#), [[arXiv:1810.09136](#)].
- [13] D. Hendrycks, M. Mazeika, and T. G. Dietterich, *Deep anomaly detection with outlier exposure*, *CoRR abs/1812.04606* (2018) [[arXiv:1812.04606](#)].
- [14] C. L. Lan and L. Dinh, *Perfect density models cannot guarantee anomaly detection*, *CoRR abs/2012.03808* (2020) [[arXiv:2012.03808](#)].
- [15] G. Kasieczka et al., *The LHC Olympics 2020 a community challenge for anomaly detection in high energy physics*, *Rept. Prog. Phys.* **84** (2021), no. 12 124201, [[arXiv:2101.08320](#)].

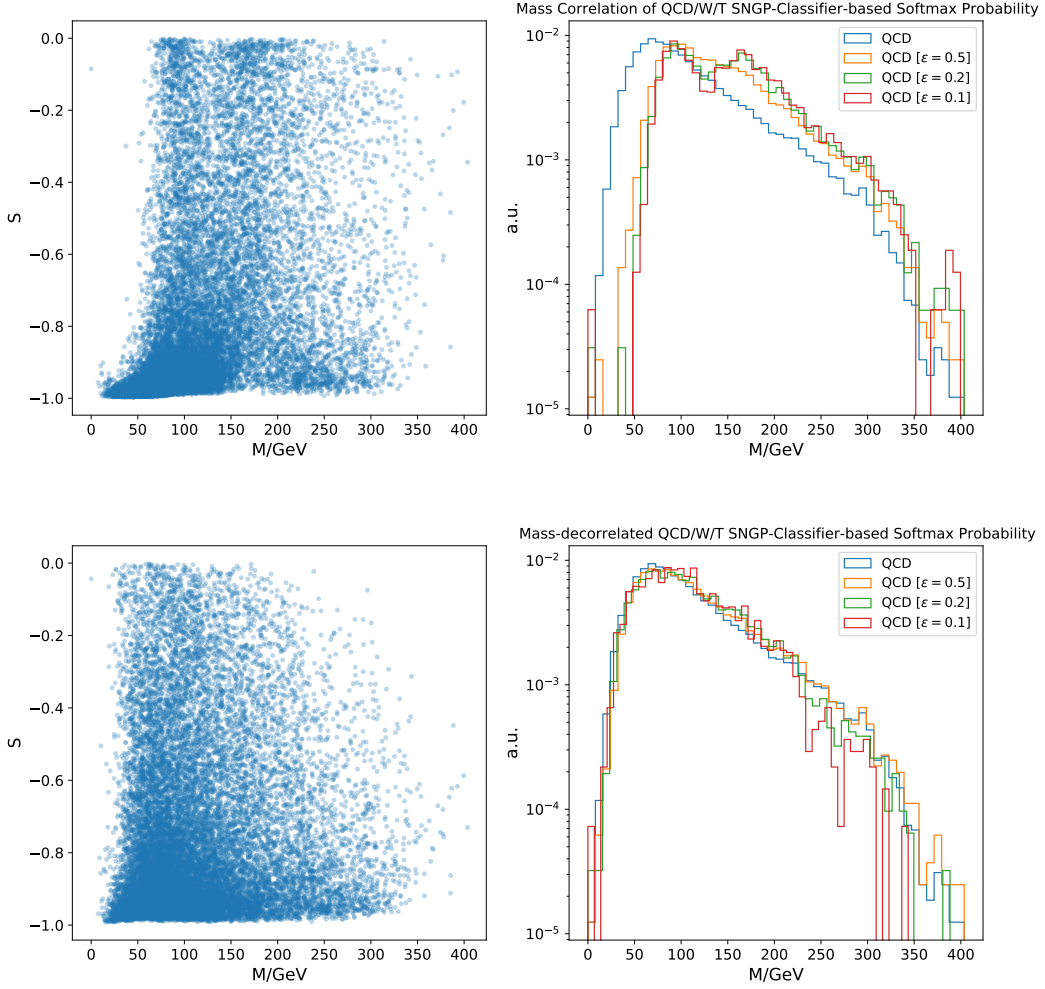


Figure 9. SNGP Model. **Top:** Un-decorrelated model in p_{QCD} . **Bottom:** Mass-decorrelated model in p_{QCD} . **Left:** Correlation between jet mass M and the anomaly score. **Right:** Mass distributions for different background acceptance rate (ϵ).

- [16] D. Hendrycks and K. Gimpel, *A baseline for detecting misclassified and out-of-distribution examples in neural networks*, *CoRR* **abs/1610.02136** (2016) [[arXiv:1610.02136](#)].
- [17] B. Lakshminarayanan, A. Pritzel, and C. Blundell, *Simple and Scalable Predictive Uncertainty Estimation using Deep Ensembles*, *arXiv e-prints* (Dec., 2016) arXiv:1612.01474, [[arXiv:1612.01474](#)].
- [18] T. DeVries and G. W. Taylor, *Learning Confidence for Out-of-Distribution Detection in Neural Networks*, *arXiv e-prints* (Feb., 2018) arXiv:1802.04865, [[arXiv:1802.04865](#)].
- [19] A. Malinin and M. Gales, *Predictive Uncertainty Estimation via Prior Networks*, *arXiv e-prints* (Feb., 2018) arXiv:1802.10501, [[arXiv:1802.10501](#)].

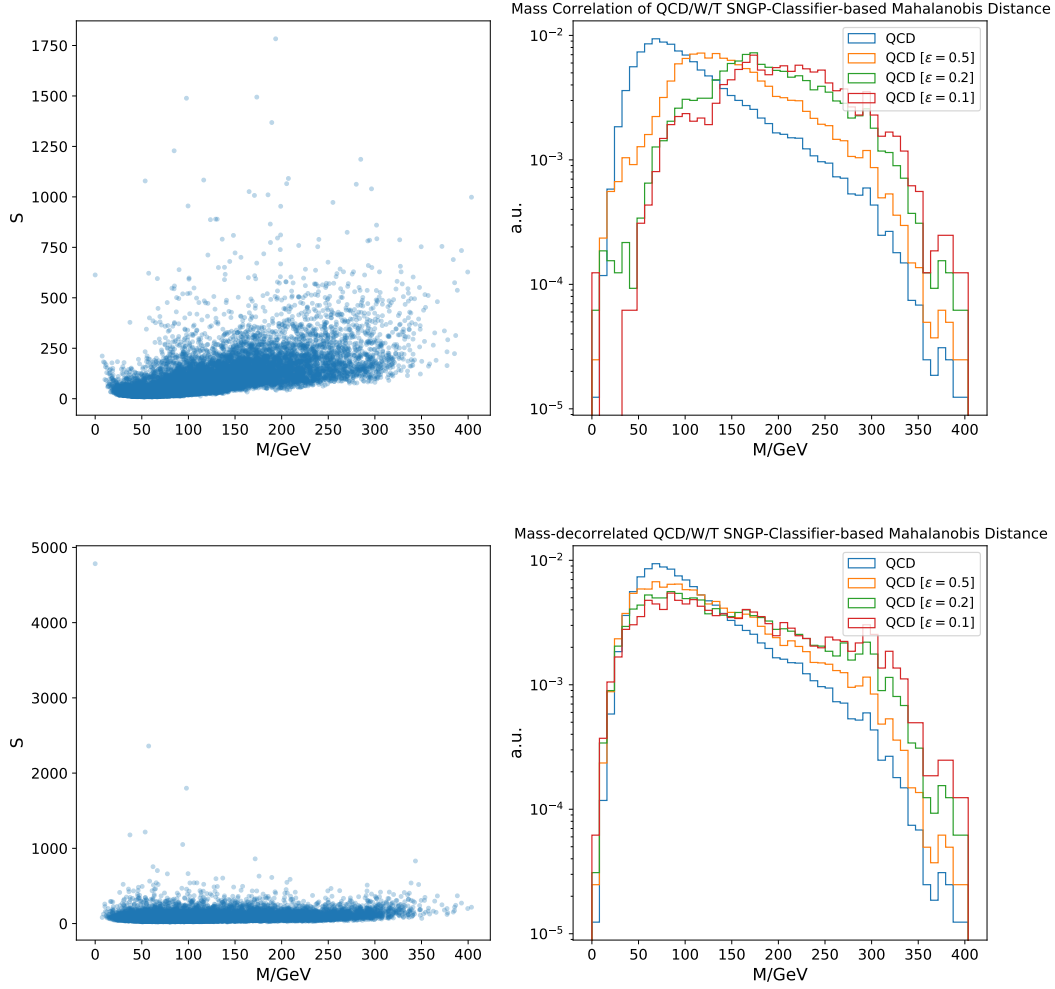


Figure 10. SNGP Model. **Top:** Un-decorrelated model in Mahalanobis distance. **Bottom:** Mass-decorrelated model in Mahalanobis distance. **Left:** Correlation between jet mass M and the anomaly score. **Right:** Mass distributions for different background acceptance rate (ϵ).

- [20] D. Macêdo, T. I. Ren, C. Zanchettin, A. L. I. Oliveira, A. Tapp, and T. B. Ludermir, *Distinction maximization loss: Fast, scalable, turnkey, and native neural networks out-of-distribution detection simply by replacing the softmax loss*, *CoRR* **abs/1908.05569** (2019) [[arXiv:1908.05569](#)].
- [21] J. van Amersfoort, L. Smith, Y. W. Teh, and Y. Gal, *Simple and scalable epistemic uncertainty estimation using a single deep deterministic neural network*, *CoRR* **abs/2003.02037** (2020) [[arXiv:2003.02037](#)].
- [22] J. Z. Liu, Z. Lin, S. Padhy, D. Tran, T. Bedrax-Weiss, and B. Lakshminarayanan, *Simple and principled uncertainty estimation with deterministic deep learning via distance awareness*, *CoRR* **abs/2006.10108** (2020) [[arXiv:2006.10108](#)].

- [23] S. Padhy, Z. Nado, J. Ren, J. Z. Liu, J. Snoek, and B. Lakshminarayanan, *Revisiting one-vs-all classifiers for predictive uncertainty and out-of-distribution detection in neural networks*, *CoRR* **abs/2007.05134** (2020) [[arXiv:2007.05134](#)].
- [24] T. Cheng, *Interpretability Study on Deep Learning for Jet Physics at the Large Hadron Collider*, in *33rd Annual Conference on Neural Information Processing Systems*, 11, 2019. [arXiv:1911.01872](#).
- [25] C. Guo, G. Pleiss, Y. Sun, and K. Q. Weinberger, *On calibration of modern neural networks*, in *Proceedings of the 34th International Conference on Machine Learning* (D. Precup and Y. W. Teh, eds.), vol. 70 of *Proceedings of Machine Learning Research*, pp. 1321–1330, PMLR, 06–11 Aug, 2017.
- [26] M. Minderer, J. Djolonga, R. Romijnders, F. A. Hubis, X. Zhai, N. Houlsby, D. Tran, and M. Lucic, *Revisiting the calibration of modern neural networks*, *ArXiv* **abs/2106.07998** (2021).
- [27] J. Dolen, P. Harris, S. Marzani, S. Rappoccio, and N. Tran, *Thinking outside the ROCs: Designing Decorrelated Taggers (DDT) for jet substructure*, *JHEP* **05** (2016) 156, [[arXiv:1603.00027](#)].
- [28] **ATLAS Collaboration** Collaboration, *Performance of mass-decorrelated jet substructure observables for hadronic two-body decay tagging in ATLAS*, Tech. Rep. ATL-PHYS-PUB-2018-014, CERN, Geneva, Jul, 2018.
- [29] L. Bradshaw, R. K. Mishra, A. Mitridate, and B. Ostdiek, *Mass Agnostic Jet Taggers*, *SciPost Phys.* **8** (2020), no. 1 011, [[arXiv:1908.08959](#)].
- [30] M. Hein, M. Andriushchenko, and J. Bitterwolf, *Why relu networks yield high-confidence predictions far away from the training data and how to mitigate the problem*, *2019 IEEE/CVF Conference on Computer Vision and Pattern Recognition (CVPR)* (2019) 41–50.
- [31] K. Lee, K. Lee, H. Lee, and J. Shin, *A simple unified framework for detecting out-of-distribution samples and adversarial attacks*, in *NeurIPS*, 2018.
- [32] J. Ren, S. Fort, J. Liu, A. G. Roy, S. Padhy, and B. Lakshminarayanan, *A simple fix to mahalanobis distance for improving near-ood detection*, *CoRR* **abs/2106.09022** (2021) [[arXiv:2106.09022](#)].
- [33] T. G. Dietterich, *Ensemble methods in machine learning*, in *Multiple Classifier Systems*, (Berlin, Heidelberg), pp. 1–15, Springer Berlin Heidelberg, 2000.
- [34] A. Niculescu-Mizil and R. Caruana, *Predicting good probabilities with supervised learning*, in *Proceedings of the 22nd International Conference on Machine Learning, ICML '05*, (New York, NY, USA), p. 625–632, Association for Computing Machinery, 2005.
- [35] Y. Gal and Z. Ghahramani, *Dropout as a bayesian approximation: Representing model uncertainty in deep learning*, 2016.
- [36] G. Franchi, A. Bursuc, E. Aldea, S. Dubuisson, and I. Bloch, *One versus all for deep neural network incertitude (OVNNI) quantification*, *CoRR* **abs/2006.00954** (2020) [[arXiv:2006.00954](#)].
- [37] C. E. Rasmussen and C. K. I. Williams, *Gaussian Processes for Machine Learning (Adaptive Computation and Machine Learning)*. The MIT Press, 2005.

- [38] T. Miyato, T. Kataoka, M. Koyama, and Y. Yoshida, *Spectral normalization for generative adversarial networks*, *CoRR* **abs/1802.05957** (2018) [[arXiv:1802.05957](#)].
- [39] J. Alwall, M. Herquet, F. Maltoni, O. Mattelaer, and T. Stelzer, *Madgraph 5: going beyond*, *Journal of High Energy Physics* **2011** (Jun, 2011).
- [40] T. Sjöstrand, S. Mrenna, and P. Skands, *A brief introduction to pythia 8.1*, *Computer Physics Communications* **178** (Jun, 2008) 852–867.
- [41] J. de Favereau, C. Delaere, P. Demin, A. Giammanco, V. Lemaître, A. Mertens, and M. Selvaggi, *Delphes 3: a modular framework for fast simulation of a generic collider experiment*, *Journal of High Energy Physics* **2014** (Feb, 2014).
- [42] M. Cacciari, G. P. Salam, and G. Soyez, *The anti-kt jet clustering algorithm*, *Journal of High Energy Physics* **2008** (Apr, 2008) 063–063.
- [43] T. Cheng, *Test sets for jet anomaly detection at the lhc*, Mar., 2021.
- [44] G. Branco, P. Ferreira, L. Lavoura, M. Rebelo, M. Sher, and J. P. Silva, *Theory and phenomenology of two-Higgs-doublet models*, *Phys. Rept.* **516** (2012) 1–102, [[arXiv:1106.0034](#)].
- [45] H. Qu and L. Gouskos, *ParticleNet: Jet Tagging via Particle Clouds*, *Phys. Rev. D* **101** (2020), no. 5 056019, [[arXiv:1902.08570](#)].
- [46] D. P. Kingma and J. Ba, *Adam: A method for stochastic optimization*, 2017.
- [47] L. N. Smith, *A disciplined approach to neural network hyper-parameters: Part 1 - learning rate, batch size, momentum, and weight decay*, *ArXiv* **abs/1803.09820** (2018).
- [48] J. Winkens, R. Bunel, A. G. Roy, R. Stanforth, V. Natarajan, J. R. Ledsam, P. MacWilliams, P. Kohli, A. Karthikesalingam, S. A. A. Kohl, taylan. cemgil, S. M. A. Eslami, and O. Ronneberger, *Contrastive training for improved out-of-distribution detection*, *ArXiv* **abs/2007.05566** (2020).
- [49] G. Kasieczka and D. Shih, *Robust Jet Classifiers through Distance Correlation*, *Phys. Rev. Lett.* **125** (2020), no. 12 122001, [[arXiv:2001.05310](#)].
- [50] J. Ren, P. J. Liu, E. Fertig, J. Snoek, R. Poplin, M. A. DePristo, J. V. Dillon, and B. Lakshminarayanan, *Likelihood ratios for out-of-distribution detection*, in *NeurIPS*, 2019.
- [51] G. Kasieczka, B. Nachman, M. D. Schwartz, and D. Shih, *Automating the ABCD method with machine learning*, *Phys. Rev. D* **103** (2021), no. 3 035021, [[arXiv:2007.14400](#)].